Engineered Science
DOI: https://dx.doi.org/10.30919/es1775

Valorization of Manganese Ore Tailings from the Borly Deposit into Functional Sorbents

Arailym Kalymbet,[1,*] Sholpan Kubekova,[1,*] Victoria Kapralova,[1] Kanay Rysbekov[1] and Silviya Lavrova,[2]

Abstract

This study reports the synthesis and characterization of a novel sorbent from manganese ore beneficiation tailings (Borly deposit, Kazakhstan), activated with 20% phosphoric acid and thermally treated at 600 °C. Compared to the raw material, the sorbent showed reduced BET surface area (6.05→3.02 m^2/g) but increased average pore diameter (13.2→21.8 nm), more negative zeta potential (−4.1→−18.9 mV), and lower water solubility (0.82%). Equilibrium tests revealed ≥99% Cu^{2+} removal and a maximum capacity of 1.329 mg/g, with a type V isotherm indicating cooperative adsorption on heterogeneous sites. Among tested models, the RALF (Redlich–Anderson–Langmuir–Freundlich) isotherm provided the best fit (R^2=0.999), confirming structured and energetically diverse adsorption sites. Kinetics followed a pseudo-second-order model (R^2≈1), suggesting chemisorption with mixed physisorption contributions, while intraparticle diffusion was not the sole rate-limiting step. Fixed-bed tests showed a dynamic capacity of 0.68 mg/g. The results highlight a sustainable approach to valorizing manganese tailings for efficient copper removal. This work demonstrates a sustainable approach to valorizing mining waste into functional sorbents for heavy metal removal. Despite their modest adsorption capacity, the materials show high removal efficiency and low cost, making them promising for polishing treatment and other cost-sensitive applications.

Keywords: Manganese tailings; Phosphate modification; Copper adsorption; RALF isotherm; Sustainable sorbent.
Received: 25 August 2025; Revised: 28 September 2025; Accepted: 01 October 2025
Article Type: Original research.

1. Introduction

Valorization of industrial waste is a relevant topic in the context of sustainable development and the transition to a green economy. This is especially relevant for Kazakhstan, whose mining enterprises annually extract millions of tons of minerals. Their enrichment and processing are accompanied by the formation of a huge volume of waste that is placed on the surface, in tailings ponds and landfills, occupying large areas of land, polluting the environment and creating long-term environmental risks.[1–4] Typically, such wastes are techno-mineral formations enriched with silicon dioxide and silicate minerals. This allows them to be used as an alternative raw material source in the processes of obtaining silicon-containing sorption materials, since the basis of most known natural and synthetic inorganic sorbents is precisely the silicate matrix.[5,6] Recently, the transformation of such mining by-products into functional materials—especially adsorbents for wastewater treatment—has garnered significant attention.[7–10]

Phosphoric acid activation combined with thermal treatment effectively restructures mineral matrices to form silicophosphate sorbents possessing abundant ion-exchange sites and porosity.[11–14] This technique has successfully transformed clay, fly ash, and mining residues into high-performance adsorbents for heavy metal ions including Cu^{2+}, Pb^{2+}, and Cd^{2+}.[15–17] Notably, phosphoric acid-activated clays demonstrated enhanced Cu^{2+} affinity due to increased surface charge.[18]

In parallel, manganese- and iron-rich wastes have been explored for arsenic removal through sorption and redox processes.[19–21] Fe/Mn oxide-coated substrates effectively immobilize As and Mn via surface complexation mechanisms.[22–24] However, studies specifically targeting manganese tailings for Cu^{2+} adsorption are scarce,[25] representing a critical research gap.

In recent years, the valorization of mining and industrial wastes into heavy-metal sorbents has rapidly advanced. Iron tailings have been transformed into magnetic nanoporous materials with high remediation potential.[26] Biogenic wastes, such as mollusk shells, were also applied as efficient adsorbents, achieving Cu^{2+} capacities up to 769 mg/g.[27] Phosphate tailings co-pyrolyzed with sewage sludge generated phosphorus-enriched biochars capable of stabilizing Zn, Pb, Mn, Ni, and Cu more effectively.[28] Moreover, mining tailings

[1]*Department of Chemical Processes and Industrial Ecology, Mining and Metallurgical Institute named after O.A. Baikonurov, Satbayev University, 22 Satbaev str., 050013, Almaty, Kazakhstan*

are increasingly recognized as a promising feedstock for the synthesis of value-added nanomaterials for environmental and technological applications.[29] These recent findings highlight the growing trend in sustainable waste-derived sorbents and reinforce the relevance of phospho-activated Borly tailings for Cu^{2+} remediation.

From our perspective, possible raw materials for obtaining such materials are waste from enrichment of manganese ores of the Republic of Kazakhstan, and, in particular, ore from the Borly deposit located in the Karaganda region. Its measured resources amount to 1088.71 thousand tons of ore with a manganese content of 13.8%. The ore is enriched by the gravity method, that is, large classes are enriched, and small classes remain in the tailings, which can lead to large losses of manganese, since the enrichment tailings are currently not utilized.

This study addresses that gap by synthesizing and characterizing a sorbent made from Borly manganese ore tailings activated with 20 wt.% phosphoric acid and calcined at 400–800 °C. The objectives are:

1. To elucidate how synthesis temperature influences phase transformation, porosity, surface charge, and structural stability;
2. To evaluate Cu^{2+} adsorption performance under static (batch), kinetic, and dynamic (fixed-bed column) conditions.

The synthesized sorbent derived from Borly manganese beneficiation tailings shows strong potential for practical application in the treatment of industrial and mining wastewaters, particularly those contaminated with copper. Such effluents are commonly generated during mineral processing, electroplating, and acid mine drainage, posing serious environmental hazards. Recent studies confirm the feasibility of converting mining waste into efficient sorbents for heavy metal removal. For example, an alkali suspension method enabled over 98% removal of Cu^{2+}, Zn^{2+}, and Cr^{3+} from copper and gold tailings leachates, demonstrating a low-cost and scalable treatment approach.[30] Technosols prepared from mining residues achieved up to 99% Cu^{2+} removal in both batch and column systems, with the metal retained mainly in stable residual forms.[31] Furthermore, sustainable approaches such as tailings repurposing and advanced dewatering for water reuse have been explored to promote circular economy practices in the mining industry.[32] These findings support the practical applicability of the developed Borly-based sorbent in fixed-bed or batch systems for the treatment of mine drainage, smelter runoff, and contaminated process waters.

The present work contributes to the sustainable valorization of mining waste by developing a scalable route to convert Borly tailings into efficient, low-cost sorbents for heavy metal remediation—supporting circular economy principles and environmental protection goals.[33]

[2]*Department of Environmental Engineering, Faculty of Chemical and System Engineering, University of Chemical Technology and Metallurgy, 8 Kliment Ohridski blvd., 1756 Sofia, Bulgaria*
[*]*E-mail*: a.kalymbet@satbayev.university (A. Kalymbet), s.kubekova@satbayev.university (S. Kubekova)

2. Materials and methods

The raw material used in this study was manganese ore beneficiation tailings collected from the Borly deposit (Karaganda region, Kazakhstan). The best surface and adsorption properties were found out to be sorbent synthesized with 20wt. % at 600°C.

2.1 Sample preparation

The thermal-acid synthesis of silicophosphate materials from ore wastes processing was carried out using varying concentrations of phosphoric acid (20 wt.%) and at calcination temperatures of 400, 600, and 800 °C. The required amount of phosphoric acid for the synthesis was then calculated based on the content of acid-sorption components. Each sample, ground to a particle size of 0–10 μm, underwent wet milling, followed by drying at 105°C for one hour and subsequent calcination at 400, 600, and 800 °C.

2.2 Characterization techniques

The phase composition of raw materials was studied using XRD, EPMA and EDXRF. XRD analysis was performed on a DRON-3 diffractometer (CuKα radiation, β-filter) under standard conditions (35 kV, 20 mA, θ–2θ mode, 2°/min). Semi-quantitative analysis was conducted using the equal hinge plate method and the PDF2 (ICDD) database. Elemental composition was determined by EPMA on a JEOL–733 microscope with an X-ray analyzer. The bulk chemical composition was analyzed using a Rigaku NEX CG II EDXRF spectrometer, employing automatic fundamental parameters correction and a helium atmosphere to enhance the detection of light elements.

Surface properties were studied using SEM (Jeol JSM-6490LA), surface area and porosity analysis (Beishide BSD-660), and zeta potential measurements (Zetasizer NanoZS 90).

The solubility of the synthesized materials was assessed by the mass loss of the products upon dissolution in water. Samples weighing 1 g, taken with an accuracy of 0.0001 g, were dissolved in 100 mL of distilled water and stirred on a shaker for 30 minutes. After that, the solution was filtered, the undissolved residue was dried and weighed. Solubility was calculated using Eq. (1) in rel. %:

$$S = \frac{(m_0 - m_1)100}{m_0} \quad (1)$$

where: S - solubility, rel. %; m_o - mass of sample before dissolution, g; m_1 - mass of a substance after dissolution, g.

The sorption behavior, including equilibrium and kinetics, was evaluated using both static and dynamic methods. Static sorption capacity at equilibrium was determined by mixing 3 g of sorbent with 100 mL of copper cation solutions at initial concentrations of 1, 10, 20, 30, and 40 mg/L. The suspensions were stirred at 200 rpm for 24 hours. After filtration, the residual Cu^{2+} concentration was measured using a double-beam atomic absorption spectrometer AA-7000 (Shimadzu). The removal efficiency (RE) (%) of the adsorbent used was

calculated using the Eq. (2):

$$RE = \frac{(C_0 - C_e)100}{C_0} \quad (2)$$

where C_o is the initial copper ions concentration and C_e is their concentration at time t in mg/L.

The adsorption capacity (mg/g) was calculated using Eq. (3) as follows:

$$q_e = \frac{(C_o - C_e)_V}{m} \quad (3)$$

where C_o and C_e are the initial and equilibrium copper ion concentrations (mg/L), respectively, V is the volume of solution (L) and m (g) is the mass of the adsorbent used.

The study evaluated the sorption kinetics of Cu^{2+} ions (initial concentration: 10 mg/L) using a batch experiment with 3 g of sorbent in 250 mL of solution agitated at 200 rpm. Samples were collected at 2, 5, 10, 30, 60, and 120 min, filtered (0.45 µm), and analyzed via AAS to determine residual Cu^{2+} concentrations.

The isotherms of Frumkin, Hill, and RALF were used for experimental equilibrium data interpretation, whereas the kinetic results were analyzed by comparative estimation of the applicability of the Pseudo-second order model, Mixed order model, and the Intraparticle diffusion model.

For dynamic sorption capacity study, a glass column (10 cm height × 1 cm diameter) was packed with 3 g of sorbent and pre-conditioned by washing with 50 mL of distilled water at a flow rate of 2 mL/min using a peristaltic pump. A Cu^{2+} solution (10 mg/L) was then continuously pumped through the column at the same flow rate. The effluent was collected in six 50 mL fractions (totaling 300 mL), and each fraction was analyzed via AAS to determine residual Cu^{2+} concentrations. All experiments were performed in triplicate, and average values were reported.

The adsorption experiments were conducted under natural pH conditions without external pH adjustment.

3. Results and discussion

3.1 Phase and elemental composition of initial waste and sorbent

X-ray diffraction (XRD) analysis (Fig. S1) revealed that the gravity separation tails from the Borly manganese ore deposit are primarily composed of quartz (SiO_2, 76.7 wt%) and kaolinite ($Al_2(Si_2O_5)(OH)_4$, 11.8 wt%). Manganese is present mainly as pyrolusite (MnO_2, 6.8 wt%), and iron as hematite (Fe_2O_3, 4.7 wt%) (Table 1). The predominance of quartz indicates a siliceous matrix with low reactivity in its native form. Fig. S1 shows the diffraction pattern of gravity-enriched manganese ore tailings, confirming the dominance of quartz.

Table 1: Semi-quantitative XRD analysis of gravity separation tails from borly.

Phase	Formula	Content (wt.%)
Quartz	SiO_2	76.7
Kaolinite	$Al_2(Si_2O_5)(OH)_4$	11.8
Pyrolusite	MnO_2	6.8
Hematite	Fe_2O_3	4.7

Electron probe microanalysis (EPMA) confirmed the high silica content, with SiO_2 averaging 79.04 wt% across multiple spectra (Table 2). Manganese is present in significant amounts (MnO: 10.51 wt%), suggesting the potential for valorization. The relatively low concentrations of Al_2O_3 (4.86 wt%) and FeO (5.23 wt%) are consistent with the observed minor kaolinite and hematite phases. The low standard deviations indicate homogeneity in composition.

Table 2: Elemental composition (wt. %) of the tailings (EPMA).

Spectrum	Al_2O_3	SiO_2	K_2O	MnO	FeO	Total
1	4.63	80.16	0.31	9.25	5.64	100
2	5.00	79.21	0.41	9.84	5.53	100
3	4.95	77.74	0.36	12.44	4.51	100
Average	4.86	79.04	0.36	10.51	5.23	100
Std. Deviation	0.20	1.22	0.05	1.69	0.63	

EDXRF analysis using the Rigaku NEX CG II system corroborated these findings (Fig. S2, Table 3). The SiO_2 content was slightly higher (80.80 wt%), while MnO (9.04 wt%) and Fe_2O_3 (4.58 wt%) were comparable to EPMA results. Trace levels of CaO, TiO_2, and P_2O_5 were also detected, indicating minor accessory minerals. Fig. S2 presents the EDXRF spectrum of the original tailings, illustrating the presence of Si, Al, Mn, and etc. Overall, the agreement between XRD, EPMA and EDXRF confirms the reliability of the compositional data and supports further modification of this waste material for environmental applications.

A number of phosphate products based on the enrichment waste of the Borly deposit ore were obtained by the acid-thermal method. The optimum synthesis temperature was determined by assessing the aqueous solubility of the synthesized materials. The results are summarized in Table 4.

The solubility values show a clear dependence on the synthesis temperature. The sample obtained at 400°C remained largely soluble (9.51%), possibly due to incomplete

Table 3: Major components in raw tailings (EDXRF).

Component	SiO_2	MnO	Al_2O_3	Fe_2O_3	P_2O_5	K_2O	CaO	TiO_2
Content (wt%)	80.80 ±0.0442	9.04 ±0.0060	4.63 ±0.0363	4.58 ±0.0039	0.17 ±0.0021	0.20 ±0.0026	0.12 ±0.0014	0.16 ±0.0011

Table 4: Influence of synthesis temperature on solubility of the synthesized materials.

Temperature, °C		
400	600	800
Solubility in water, rel. %		
9.51±0,12	0.82±0,03	4.41±0,03

condensation of the phosphate matrix and the presence of soluble substances such as aluminum and manganese dihydrogen phosphates. The material synthesized at 600°C showed the lowest solubility (0.82%), since an increase in temperature to 600°C intensifies the dehydration process and leads to the formation of insoluble crystalline condensed phosphates of these elements. An increase in temperature also promotes the incorporation of PO_4 tetrahedra into the silicate matrix, leading to a decrease in the solubility of the synthesized product. A further increase in temperature to 800°C possibly leads to the formation of less stable glassy phases, causing some increase in the solubility of this product (4.41%).[14] These results confirm that the optimal temperature for obtaining chemically stable sorbents with minimal solubility in water is 600 °C.

After chemical modification with phosphoric acid and thermal activation, EDXRF analysis revealed an increase in phosphorus content (P_2O_5: 2.57 wt%), indicating the successful incorporation of phosphate groups into the solid matrix (Fig. S3, Table 5). Fig. S3 demonstrates the EDXRF spectrum of the sorbent synthesized with 20 wt.% H_3PO_4 at 600 °C, where an increased phosphorus signal confirms successful surface modification. This may enhance the surface reactivity of the material and the metal-binding capacity. SiO_2 remained the dominant phase with minor changes in other oxides.

3.2 SEM Morphology and Surface Characteristics

The Scanning Electron Microscopy (SEM) analysis revealed pronounced morphological transformations resulting from acid modification and thermal activation. The raw tailings (Fig. 1a–b) exhibited angular, densely packed particles with smooth surfaces, indicative of a compact, low-reactivity structure. In contrast, the synthesized sorbent (Fig. 1c–d), prepared using 20 wt.% phosphoric acid and treated at 600 °C, displayed a highly porous, aggregated morphology characterized by irregular microcracks and increased surface roughness. This microstructural evolution significantly enhances surface area and accessibility of active sites, which is advantageous for metal ion sorption.

Despite a reduction in surface area and pore volume after phosphoric acid modification and thermal treatment, the average pore diameter increased significantly from 13.2 nm to 21.8 nm, suggesting partial collapse or restructuring of smaller pores into larger mesopores (Table 6).

The shift toward more negative zeta potential can be attributed to the formation of amorphous phosphate phases enriched with $–PO_4^{2-}$ and –OH groups, which partially dissociate in aqueous solution, thereby increasing the density of negative surface charges. Thermal activation further stabilizes these groups by restructuring the mineral matrix and removing soluble phases, while partial immobilization of native cations (*e. g*, Mn^{2+}, Ca^{2+}) reduces charge screening. As a result, the net negative potential is enhanced, strengthening electrostatic affinity toward cationic species such as Cu^{2+}. Similar mechanisms have been reported for phosphate-modified biochars, where increased abundance of surface phosphate and hydroxyl groups after calcination led to more negative zeta potentials and improved sorption of heavy metals.[34,35]

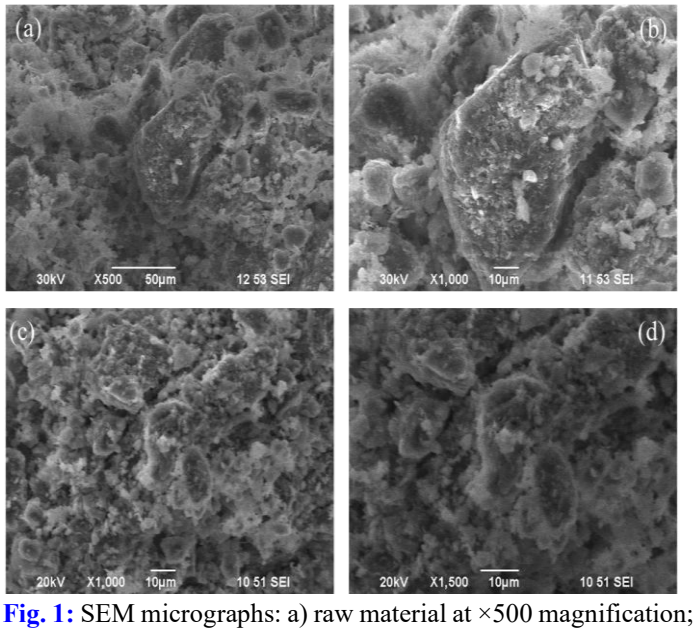

Fig. 1: SEM micrographs: a) raw material at ×500 magnification; b) raw material at ×1000; c) synthesized sorbent at ×1000; d) synthesized sorbent at ×1500.

Thus, while the specific surface area decreased, the increase in mesoporosity and surface charge density could synergistically contribute to improved sorption performance, particularly in systems dominated by electrostatic interactions. More data on sorbents synthesized at 400 °C and 800 °C are available in the Supplementary Materials (Fig. S4, Table S1).

On Fig. S4 and Table S1, could be seen the loose, underdeveloped structure with low surface area (BET: 2.34 m^2/g) and small pore volume (0.0128 cm^3/g) of the sorbent synthesized at 400 °C, indicating insufficient activation. In contrast, the sample obtained at 800 °C is denser, with glassy needle-like formations and larger pores (30.8 nm), but a less negative zeta potential (−12.7 mV), suggesting reduced surface charge.

These observations support that 600 °C provides optimal structural development and surface activation without excessive densification, resulting in higher sorption efficiency. In addition to the average pore diameters derived from BET analysis, the BJH pore size distribution of the sorbent

Table 5: Major components in modified material (sorbent synthesized with 20wt. % H_3PO_4 at 600°C) (EDXRF).

Component	SiO_2	MnO	Al_2O_3	Fe_2O_3	P_2O_5	K_2O	CaO	TiO_2
Content (wt%)	78.80 ±0.0473	9.26 ±0.0065	4.70 ±0.0364	3.93 ±0.0038	2.57 ±0.0076	0.239 ±0.0026	0.12 ±0.0015	0.13 ±0.0010

Table 6: Surface characteristics and charge of raw material and sorbent.

Parameter	BET Surface Area (m^2/g)	Langmuir Surface Area (m^2/g)	D-R Micropore Area (m^2/g)	Total Pore Volume (cm^3/g)	Average Pore Diameter (nm)	BJH Desorption Area (m^2/g)	BJH Pore Volume (cm^3/g)	Zeta potential (mV)
Raw material	6.0532	9.4777	6.8211	0.0200	13.2162	6.3243	0.0194	-4.12
Synthesized sorbent	3.0220	4.6979	3.4830	0.0165	21.8398	3.5244	0.0160	-18.9

synthesized with 20 wt.% H_3PO_4 at 600 °C is presented in Fig. S5 (Supplementary Material). The distribution confirms the predominance of mesopores, supporting the SEM observations of a porous surface morphology.

3.3 Equilibrium and kinetics of the sorption process of copper cations

The synthesized at 600 °C using 20 wt.% phosphoric acid adsorbent showed the best physicochemical characteristics, including improved surface accessibility and more uniform pore distribution. These properties contributed to its significant sorption performance, which was evaluated under both static (batch) and dynamic (fixed-bed column) conditions.

3.3.1 Equilibrium sorption studies

Batch adsorption experiments were conducted to evaluate the equilibrium adsorption capacity (q_e) and copper removal efficiency (RE) of the synthesized sorbent. The experimental study was carried out by contacting 100 mL of aqueous copper ion solutions (1-40 mg/L) with 3.0 g of adsorbent. No pH buffering was applied, and the initial pH of the systems varied naturally between 4.5 and 6.0. After reaching the equilibrium, the residual Cu^{2+} concentration (C_e) was measured, and the results are presented in Table 7.

Table 7: Equilibrium removal of Cu^{2+} by the synthesized sorbent (20 wt.% H_3PO_4, 600 °C), the value of the residual concentration is given by calculating the average value from three experiments.

C_o (mg/L)	C_e (mg/L)	RE (%)	q_e (mg/g)
0	0	0	0
1	0.010	99.00	0.033
10	0.026	99.75	0.332
20	0.043	99.78	0.665
30	0.068	99.77	0.998
40	0.132	99.67	1.329

The synthesized sorbent demonstrated excellent Cu^{2+} removal efficiency (≥99%) across all tested concentrations, with q_e increasing from 0.033 to 1.329 mg/g as C_o increased. Notably, even at 40 mg/L, the sorbent retained high removal performance, indicating strong affinity for Cu^{2+} and effective active site availability under equilibrium conditions.

By comparing the experimental isotherm to the IUPAC classification of adsorption isotherms,[36] the data were found to correspond to a type V isotherm, characterized by an S-shaped (sigmoidal) profile. This shape typically indicates cooperative adsorption behavior and surface heterogeneity. To interpret the equilibrium data and gain insights into the underlying adsorption mechanisms, three nonlinear isotherm models were applied (Table S2): the Frumkin, Rigid Adsorbent Lattice Fluid (RALF), and Hill models.[36–39]

The nonlinear expressions of the referenced models have been simplified to support their practical implementation in curve-fitting applications.[36,40,41] Using standard statistical criteria like R^2, SSE, MSE, and RMSE, the model fit quality was assessed (Table 8).

Table 8: Isotherm model parameters and error function values for Cu^{2+} adsorption onto thermally treated adsorbent.

System	Coper ions – Synthesized adsorbent 600°C			
Equilibrium model	Model parameters		Error function	
Frumkin	q_{max}	1.227	R^2	0.892
	K	5.934	SSE	0.030
	a	2.894	MSE	0.006
			RMSE	0.078
RALF	q_{max}	1.345	R^2	0.999
	K	120.343	SSE	0.002
	a	1.659	MSE	0.001
			RMSE	0.028
Hill	q_{max}	1.497	R^2	1.000
	K	484.078	SSE	0.001
	n	2.040	MSE	0.000
			RMSE	0.016

The Frumkin isotherm, which incorporates lateral interactions among adsorbed species, yielded an interaction

parameter of a=2.894, indicating attractive interaction (a>0). Despite this, its overall fit to the experimental data was limited (R^2=0.892; RMSE=0.078), likely due to its underlying assumptions of a homogeneous adsorption surface and constant heat of adsorption, which may not reflect the complexity of the synthesized material. In contrast, the Rigid Adsorbent Lattice Fluid (RALF) model, which integrates both molecular packing constraints and surface heterogeneity, demonstrated a markedly improved fit (R^2=0.999; RMSE=0.028). This suggests that the sorbent possesses structured and energetically diverse adsorption sites, consistent with thermally modified surfaces. The Hill isotherm further supported the presence of strong cooperative adsorption behavior (n=2.040) and produced an exceptional statistical fit (R^2=1.000; RMSE=0.016); however, its empirical nature limits mechanistic interpretation.

Notably, all models estimated similar maximum adsorption capacities (1.2-1.5 mg/g), reinforcing the reliability of the experimental data. Overall, the RALF model offers the most comprehensive description of copper ion adsorption onto the synthesized sorbent, combining mechanistic validity with excellent statistical performance, whereas simpler models like Frumkin fall short of explaining the full complexity of the adsorption process. Fig. 2 presents the fitted isotherm models in comparison with the experimental data.

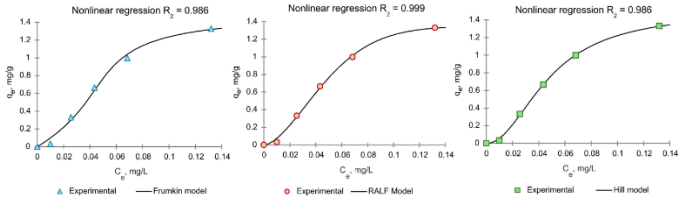

Fig. 2: Experimental equilibrium data interpretation using models proper for type V isotherm.

Among the applied models, the superior performance of the RALF isotherm can be rationalized by its solid theoretical foundation. Unlike empirical or semi-empirical approaches, RALF is rooted in statistical thermodynamics and explicitly accounts for molecular packing constraints within a lattice framework, as well as the energetic heterogeneity of adsorption sites.[42,43] This makes it particularly suitable for describing sorbents with structurally modified surfaces, such as the thermally treated silicophosphate material in this study, where both amorphous and crystalline domains contribute to adsorption. Furthermore, the RALF model captures cooperative adsorption effects arising from interactions between adsorbed ions, offering a mechanistic explanation for the characteristic sigmoidal shape of the experimental isotherm, while maintaining excellent statistical fit to the experimental data.

This data supports the sorbent's applicability for treating aqueous systems contaminated with varying levels of copper ions, showing favorable performance without the need for pH control agents.

3.3.2 Sorption kinetics

Kinetic experiments were conducted to assess the rate and mechanism of Cu^{2+} ion sorption at an initial concentration (C_0) of 10 mg/L. Batch experiments were carried out using 3 g of sorbent in 250 mL of Cu^{2+} solution under constant agitation at 200 rpm. At predetermined time (t) intervals (2, 5, 10, 30, 60, and 120 minutes), aliquots were taken, filtered through 0.45 µm membranes, and analyzed by atomic absorption spectroscopy (AAS) to determine the residual Cu^{2+} concentrations (C_t). The experimental data are summarized in Table 9.

Table 9: Kinetic parameters of Cu^{2+} adsorption on the synthesized adsorbent, the value of the residual concentration is given by calculating the average value from three experiments.

Time (min)	Ct, mg/L	RE (%)	q_t (mg/g)
0	10.000	0.00	0.000
2	0.298	97.02	0.809
5	0.254	97.46	0.812
10	0.209	97.91	0.816
30	0.155	98.45	0.820
60	0.073	98.82	0.824
120	0.118	99.27	0.827

The experimental data shows a rapid initial uptake, with 97 % of the equilibrium capacity (0.809 mg/g) reached within 2 minutes, followed by a gradual approach to saturation, achieving a final capacity of 0.827 mg/g (99.27% removal efficiency) at 120 minutes. The adsorption capacity gradually increased with time, reaching near-equilibrium conditions after 30 minutes. The maximum adsorption capacity of 0.83 mg/g was achieved in 2 hours.

The process of adsorption on porous solid adsorbents typically includes four main stages. The first stage is bulk transport of adsorbate molecules from the solution volume to the adsorbent particle. The second stage is external diffusion through the boundary layer surrounding the particle. The third stage is intraparticle diffusion into the pore space. The final stage is adsorption on active centers of the adsorbent surface.[44] Analysis of experimental data using four kinetic models (pseudo-second order, mixed pseudo-first/pseudo-second order, Elovich model and intraparticle diffusion model) allowed to identify the limiting stages of the process. The results are presented in Table 10.

The pseudo-second order (PSO) model showed an excellent fit to the experimental data (Fig. 3a, Table 10), with predicted q_e values closely matching the measured capacity ($R^2 \approx 1$). This indicates chemisorption as the dominant rate-controlling step, likely via electron sharing or exchange, and the high k_2 reflects a strong initial driving force. The mixed-order model also fits well, capturing the shift from rapid uptake to slower equilibrium, suggesting a combination of physisorption at early stages and chemisorption near equilibrium.

Table 10: Adsorption kinetic model rate constants for Cu (II) adsorption onto synthesized adsorbent.

Model	Parameter		Error	
Pseudo-second order model			R^2	0.9999
	k_2	0.822696	SSE	0.0001
	$q_{e\ calc}$	29.76687	MSE	0.0000
			RMSE	0.0034
Mixed-order model	k_1	-0.149	R^2	0.9999
	f_2	1.007	SSE	0.0000
	k_2	$0.2587x10^2$	MSE	0.0000
			RMSE	0.0040
Elovich model	α	6.6217	R^2	0.3798
	β	9.3191	MSE	0.0711
			RMSE	0.2677
Intraparticle diffusion model	k_{i1}	0.0417	R_{i1}^2	0.2725
	C_{i1}	0.5164		

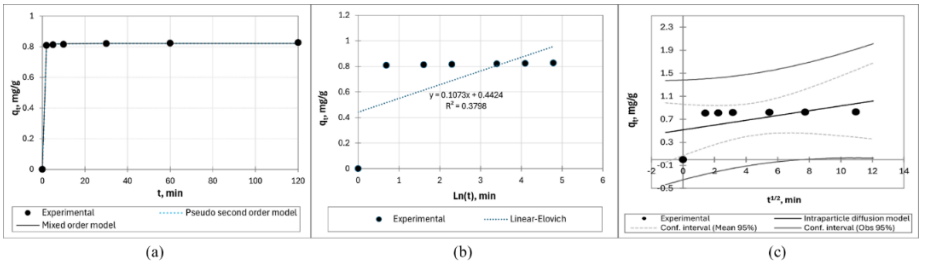

(a) (b) (c)

Fig. 3: Experimental data and kinetic models for the system "synthesized adsorbent - copper ions".

Table 11: Dynamic Cu^{2+} sorption performance, the value of the residual concentration is given by calculating the average value from three experiments.

Fraction	Effluent Volume (mL)	Residual Cu^{2+} (mg/L)	Cu^{2+} Removed (mg)	Cu^{2+} Removed (mmol)	Cumulative Cu^{2+} Removed (mg)	RE (%)	q_e (mg/g)
1	50	5.968	0.402	0.006	0.402	40.30	0.134
2	50	6.996	0.350	0.006	0.752	30.00	0.251
3	50	7.062	0.347	0.006	1.099	29.40	0.366
4	50	8.924	0.254	0.004	1.353	10.80	0.451
5	50	7.557	0.372	0.006	1.725	24.40	0.575
6	50	8.109	0.320	0.005	2.044	18.90	0.681

The Elovich model, commonly used for chemisorption on heterogeneous surfaces, showed a poor fit (R^2=0.3798, Fig. 3b). Despite this, the high initial adsorption rate (α=6.62 mg/g·min) and removal efficiency (~97% in the first interval) indicate rapid site saturation, with β=9.32 g/mg suggesting a slower rate increase over time. Such behavior may result from fast binding by chemisorption, physisorption, or film diffusion. Thus, the model serves as a diagnostic tool rather than proof of chemisorption. If the intraparticle diffusion governs the adsorption process, a plot of q_t vs. $t^{1/2}$ should yield a straight line. Furthermore, if this line passes through the origin, intraparticle diffusion can be considered the sole rate-limiting step. In contrast, deviation from the origin indicates the involvement of additional mechanisms alongside intraparticle diffusion.[45,46] As shown in Fig. 3c and Table 10, the plot does not intersect the origin (C_{i1}=0.5164 m/g, *i. e.*, intercept ≠ 0), and the regression coefficient is notably low (R^2=0.2725). The intraparticle diffusion rate constant is also relatively small (k_{i1}=0.0417 mg/g.$min^{1/2}$), indicating slow diffusion into the pores. These results suggest that intraparticle diffusion is not the dominant adsorption step. Instead, the adsorption process appears to be governed by a mixed-control mechanism, with the primary rate limitation likely arising from boundary layer effects and surface interactions rather than pore diffusion.

3.3.3 Dynamic sorption (Fixed-Bed Column)

Dynamic sorption experiments were conducted using a fixed-bed column setup to evaluate sorption performance under continuous flow conditions. A glass column (10 cm height × 10 mm inner diameter) was packed with 3 g of sorbent and pre-conditioned by passing 50 mL of distilled water through the bed at a flow rate of 2 mL/min using a peristaltic pump. Subsequently, a Cu^{2+} solution (10 mg/L) was continuously pumped through the column at the same flow rate. The effluent

was collected in six successive 50 mL fractions (total volume: 300 mL), and residual Cu^{2+} concentrations in each fraction were determined using atomic absorption spectroscopy (AAS). The results are summarized in Table 11.

The fixed-bed column experiment was conducted to evaluate the Cu^{2+} removal efficiency and sorption capacity of the synthesized sorbent under continuous flow conditions. As presented in Table 11, the influent Cu^{2+} concentration was maintained at 10 mg/L, and the effluent was collected in six successive 50 mL fractions.

The initial fraction (fraction 0) contained a high concentration of 22.14 mg/L due to the pre-conditioning process and displacement of unadsorbed Cu^{2+} from void spaces. Starting from fraction 1, the Cu^{2+} concentration in the effluent ranged between 5.97 and 8.92 mg/L, indicating partial retention of Cu^{2+} ions by the sorbent throughout the flow process.

The highest Cu^{2+} removal efficiency (RE) was observed in the first collected fraction (40.3%), which gradually declined in subsequent fractions. This decrease can be attributed to the progressive saturation of active sites on the sorbent surface. The cumulative dynamic sorption capacity (q_e) reached 0.681 mg/g by the sixth fraction, indicating moderate binding of copper ions under flow conditions.

The silicophosphate sorbent synthesized from mining waste in this study shows a lower equilibrium capacity (1.329 mg/g) compared to other biochar-based sorbents,[47–51] but remains competitive due to its low-cost raw materials, high chemical stability, and the presence of specific ion-exchange sites. Moreover, while the maximum removal efficiency under dynamic column operation reached 40.3% in the first collected fraction and gradually decreased in subsequent fractions, this performance highlights the practical applicability of the material under flow-through conditions, which are more relevant for real wastewater treatment compared to equilibrium batch tests (Fig. 4).

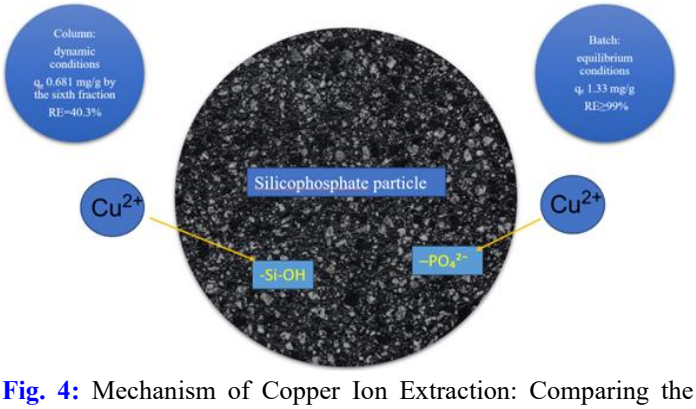

Fig. 4: Mechanism of Copper Ion Extraction: Comparing the efficiency of dynamic and batch adsorption.

Overall, the synthesized sorbent demonstrated a continuous but limited uptake of Cu^{2+} ions during the column operation. The breakthrough occurred early, suggesting a relatively low affinity or limited number of active binding sites under dynamic conditions, which contrasts with the higher removal efficiency observed under batch conditions. Nevertheless, the material still holds potential for polishing applications or secondary treatment where moderate Cu^{2+} concentrations persist.

4. Conclusion

Phosphate-modified Borly manganese tailings (600 °C) formed an amorphous phosphate phase with restructured pores and a strongly negative surface charge, enhancing Cu^{2+} uptake. Adsorption followed a type V isotherm best described by the RALF model and pseudo-second-order kinetics, indicating heterogeneous sites and chemisorption with physisorption contributions. These structural and surface features enabled high capacity and rapid removal under both batch and dynamic conditions.

Although the sorbent showed excellent removal efficiency (≥99%), its equilibrium adsorption capacity (≈1.3 mg/g) is relatively low compared to many reported materials. This suggests its best use is in polishing or secondary treatment, where its low cost, abundance, and sustainable origin provide clear advantages.

Overall, the results highlight that waste-derived phosphate-modified materials represent a sustainable and economically viable pathway for the development of high-performance sorbents for heavy metal removal. Their low-cost origin from abundant mining residues, combined with simple synthesis involving acid treatment and thermal activation, makes them attractive for scalable industrial applications in wastewater treatment. Beyond copper, such materials hold promise for removing other hazardous metal ions (e.g., Cd^{2+}, Co^{2+}, Ni^{2+}), offering broad environmental protection. Future research should focus not only on real effluent applications but also on the regeneration, reuse, and lifecycle assessment of these sorbents to confirm their long-term practicality and contribution to sustainable resource management.

Acknowledgments

This research has been funded by the Committee of Science of the Ministry of Science and Higher Education of the Republic of Kazakhstan (Grant No. BR21881939).

Conflict of Interest

There is no conflict of interest.

Supporting Information

Applicable.

CRediT Statement

Sholpan Kubekova, Victoria Kapralova, Kanay Rysbekov and Silviya Lavrova: Conceptualization; **Silviya Lavrova:** Formal analysis; **Kanay Rysbekov:** Funding acquisition; **Arailym Kalymbet:** Investigation; **Sholpan Kubekova, Victoria Kapralova and Silviya Lavrova:** Methodology;

Arailym Kalymbet, Kanay Rysbekov: Project administration; **Sholpan Kubekova and Victoria Kapralova:** Resources; **Arailym Kalymbet and Silviya Lavrova:** Software; **Sholpan Kubekova and Arailym Kalymbet:** Supervision; **Arailym Kalymbet, Sholpan Kubekova, Victoria Kapralova, Kanay Rysbekov and Silviya Lavrova:** Validation; **Arailym Kalymbet and Silviya Lavrova:** Visualization; **Arailym Kalymbet, Sholpan Kubekova and Victoria Kapralova:** Writing—Original draft preparation; **Arailym Kalymbet and Silviya Lavrova:** Writing—review and editing; All authors have read and agreed to the published version of the manuscript.

References

[1] M. Nurpeissova, M. Zh. Bitimbayev, K. B. Rysbekov, *et al*., Geodetic substantiation of the Saryarka Copper ore region, *News of National Academy of Sciences of the Republic of Kazakhstan*, 2020, **6**(444), 194–202, doi: 10.32014/2020.2518-170X.147.

[2] D.-M. Xu, C.-L. Zhan, H.-X. Liu, H.-Z. Lin, A critical review on environmental implications, recycling strategies, and ecological remediation for mine tailings, *Environmental Science and Pollution Research*, 2019, **26**, 35657-35669, doi: 10.1007/s11356-019-06555-3.

[3] P. Saik, O. Cherniaiev, O. Anisimov, K. Rysbekov, Substantiation of the direction for mining operations that develop under conditions of shear processes caused by hydrostatic pressure, *Sustainability*, 2023, **15**(22), 15690, doi: 10.3390/su152215690.

[4] M. Kunarbekova, Y. Yeszhan, S. Zharylkan, M. Alipuly, U. Zhantikeyev, A. Beisebayeva, K. Kudaibergenov, K. Rysbekov, Z. Toktarbay, S. Azat, The state of the art of the mining and metallurgical industry in Kazakhstan and future perspectives: a systematic review, *ES Materials & Manufacturing*, 2024, **25**, doi: 10.30919/esmm1219.

[5] B. Bal, S. Ghosh, A. P. Das, Microbial recovery and recycling of manganese waste and their future application: a review, *Geomicrobiology Journal*, 2019, **36**, 85-96, doi: 10.1080/01490451.2018.1497731.

[6] K. Liu, H. Zhang, Y. Liu, Y. Li, F. Yu, Investigation of plant species and their heavy metal accumulation in manganese mine tailings in Pingle Mn mine, China, *Environmental Science and Pollution Research*, 2020, **27**, 19933-19945, doi: 10.1007/s11356-020-08514-9.

[7] Z. Chen, W. Wei, H. Chen, B.-J. Ni, Recent advances in waste-derived functional materials for wastewater remediation, *Eco-Environment & Health*, 2022, **1**, 86-104, doi: 10.1016/j.eehl.2022.05.001.

[8] D. Bolaños Guerrón, J. Capa, L. C. Flores, Retention of heavy metals from mine tailings using Technosols prepared with native soils and nanoparticles, *Heliyon*, 2021, **7**, e07631, doi: 10.1016/j.heliyon.2021.e07631.

[9] O. Carmignano, S. Vieira, A. P. Teixeira, F. Lameiras, P. R. Brandão, R. Lago, Iron ore tailings: characterization and applications, *Journal of the Brazilian Chemical Society*, 2021, **32**, 1895-1911, doi: 10.21577/0103-5053.20210100.

[10] S. L. Kim, H. Yang, S. Lee, S.-K. Cho, C.-G. Lee, S. Azat, J. Lee, Mining waste as heterogeneous catalysts, *Green Chemistry*, 2025, **29**, 8691-8709, doi: 10.1039/d5gc01509j.

[11] K. S. Sopanrao, A. Venugopal, C. M. Patel, I. Sreedhar, Phosphoric acid–modified bentonite-chitosan composite beads: a novel and cost-effective adsorbent for multi-metal wastewater treatment, *Environmental Science and Pollution Research*, 2024, doi: 10.1007/s11356-024-35653-0.

[12] T. K. Sen, Agricultural solid wastes based adsorbent materials in the remediation of heavy metal ions from water and wastewater by adsorption: a review, *Molecules*, 2023, **28**(14), 5575, doi: 10.3390/molecules28145575.

[13] M. Fomina, G. M. Gadd, Biosorption: current perspectives on concept, definition and application, *Bioresource Technology*, 2014, **160**, 3-14, doi: 10.1016/j.biortech.2013.12.102.

[14] S. N. Kubekova, V. I. Kapralova, and S. A. Telkov, Silicophosphate Sorbents, Based on Ore-Processing Plants' Waste in Kazakhstan., *International Journal of Environmental and Science Education*, 2016, **11**, 4985–4996.

[15] M. Hassan, R. Naidu, J. Du, Y. Liu, F. Qi, Critical review of magnetic biosorbents: their preparation, application, and regeneration for wastewater treatment, *Science of The Total Environment*, 2020, **702**, 134893, doi: 10.1016/j.scitotenv.2019.134893.

[16] H. Cui, Z. Xu, T. Guo, S. Hu, R. Xia, S. Zhang, Y. Wang, J. Zhou, Calcium hydroxide–phosphate-modified fly ash enhances the adsorption and stabilization of soil lead and cadmium, *Agronomy*, 2024, **14**(12), 2905, doi: 10.3390/agronomy14122905.

[17] T. Bao, M. M. Damtie, C. Y. Wang, Z. Chen, Q. Tao, W. Wei, K. Cho, P. Yuan, R. L. Frost, B.-J. Ni, Comprehensive review of modified clay minerals for phosphate management and future prospects, *Journal of Cleaner Production*, 2024, **447**, 141425, doi: 10.1016/j.jclepro.2024.141425.

[18] M. Djebbar, F. Djafri, Adsorption of Cu(II) on natural and treated clays, *Water Quality Research Journal*, 2016, **51**, 26-32, doi: 10.2166/wqrjc.2015.051.

[19] Y. Li, Z. Xu, H. Ma, A. S. Hursthouse, Removal of manganese(II) from acid mine wastewater: a review of the challenges and opportunities with special emphasis on Mn-oxidizing bacteria and microalgae, *Water*, 2019, **11**(12), 2493, doi: 10.3390/w11122493.

[20] A. Segues Codina, N. Sergienko, C. M. Borrego, J. Radjenovic, Manganese oxide-functionalized graphene sponge electrodes for electrochemical chlorine-free disinfection of tap water, *Chemical Engineering Journal*, 2023, **472**, 145082, doi: 10.1016/j.cej.2023.145082.

[21] M. A. Islam, D. W. Morton, B. B. Johnson, B. Mainali, M. J. Angove, Manganese oxides and their application to metal ion and contaminant removal from wastewater, *Journal of Water Process Engineering*, 2018, **26**, 264-280, doi: 10.1016/j.jwpe.2018.10.018.

[22] M. Younas, A. U. R. Bacha, K. Khan, I. Nabi, Z. Ullah, M. Humayun, J. Hou, Application of manganese oxide-based

materials for arsenic removal: a review, *Science of The Total Environment*, 2024, **918**, 170269, doi: 10.1016/j.scitotenv.2024.170269.
[23] R. El Haouti, Z. Anfar, S. Et-Taleb, M. Benafqir, S. Lhanafi, N. El Alem, Removal of heavy metals and organic pollutants by a sand rich in iron oxide, *Euro-Mediterranean Journal for Environmental Integration*, 2018, **3**(17) doi: 10.1007/s41207-018-0058-9.
[24] C.-M. Chon, D.-W. Cho, I.-H. Nam, J.-G. Kim, H. Song, Fabrication of Fe/Mn oxide composite adsorbents for adsorptive removal of zinc and phosphate, *Journal of Soils and Sediments*, 2018, **18**, 946-956, doi: 10.1007/s11368-017-1784-3.
[25] L. Velarde, M. S. Nabavi, E. Escalera, M.-L. Antti, F. Akhtar, Adsorption of heavy metals on natural zeolites: a review, *Chemosphere*, 2023, **328**, 138508, doi: 10.1016/j.chemosphere.2023.138508.
[26] C. Xu, Y. Feng, H. Li, R. Wu, J. Ju, S. Liu, Y. Yang, B. Wang, Adsorption of heavy metal ions by iron tailings: Behavior, mechanism, evaluation and new perspectives, *Journal of Cleaner Production*, 2022, **344**, 131065, doi: 10.1016/j.jclepro.2022.131065.
[27] B. Fernández Pérez, J. Ayala Espina, M. L. Á. Fernández González, Adsorption of heavy metals ions from mining metallurgical tailings leachate using a shell-based adsorbent: characterization, kinetics and isotherm studies, *Materials (basel)*, 2022, **15**, 5315, doi: 10.3390/ma15155315.
[28] Y. Xiao, T. Yan, P. Yao, W. Xiang, Y. Wu, J. Li, Co-pyrolysis of sewage sludge and phosphate tailings: Synergistically enhancing heavy metal immobilization and phosphorus availability, *Waste Management*, 2024, **181**, 44-56, doi: 10.1016/j.wasman.2024.04.003.
[29] F. Pizarro Barraza, D. Thiyagarajan, A. Ramadoss, V. S. Manikandan, S. S. Dhanabalan, C. V. Abarzúa, P. Sotomayor Soloaga, J. Campos Nazer, M. J. Morel, A. Thirumurugan, Unlocking the potential: Mining tailings as a source of sustainable nanomaterials, *Renewable and Sustainable Energy Reviews*, 2024, **202**, 114665, doi: 10.1016/j.rser.2024.114665.
[30] S. Jiang, Y. Chen, S. Chen, Z. Hu, Removal and reclamation of trace metals from copper and gold mine tailing leachates using an alkali suspension method, *Water*, 2023, **15**, 1902, doi: 10.3390/w15101902.
[31] F. Perlatti, F. Ruiz, X. L. Otero, T. O. Ferreira, Adsorption and sequential extraction of copper in technosols prepared from unconsolidated mining wastes rich in limestone, bentonite, and organic matter, *Mining*, 2023, **3**(1), 151-162, doi: 10.3390/mining3010009.
[32] L. Hamraoui, A. Bergani, M. Ettoumi, A. Aboulaich, Y. Taha, A. Khalil, C. M. Neculita, M. Benzaazoua, Towards a circular economy in the mining industry: possible solutions for water recovery through advanced mineral tailings dewatering, *Minerals*, 2024, **14**(3), 319, doi: 10.3390/min14030319.
[33] European Commission. Directorate General for Communication., Circular Economy Action Plan: the European Green Deal., 2020.
[34] Y. Zeng, Y. Lin, M. Ma, H. Chen, A review on the removal of heavy metals from water by phosphorus-enriched biochar, *Minerals*, 2024, **14**(1), 61, doi: 10.3390/min14010061.
[35] H. Zhang, J. Shao, S. Zhang, X. Zhang, H. Chen, Effect of phosphorus-modified biochars on immobilization of Cu (II), Cd (II), and as (V) in paddy soil, *Journal of Hazardous Materials*, 2020, **390**, 121349, doi: 10.1016/j.jhazmat.2019.121349.
[36] M. A. Al-Ghouti, D. A. Da'ana, Guidelines for the use and interpretation of adsorption isotherm models: a review, *Journal of Hazardous Materials*, 2020, **393**, 122383, doi: 10.1016/j.jhazmat.2020.122383.
[37] C. Buttersack, Modeling of type IV and V sigmoidal adsorption isotherms, *Physical Chemistry Chemical Physics*, 2019, **10**, 5614-5626, doi: 10.1039/c8cp07751g.
[38] M. C. Verbraeken, S. Brandani, A priori predictions of type I and type V isotherms by the rigid adsorbent lattice fluid, *Adsorption*, 2020, **26**, 989-1000, doi: 10.1007/s10450-019-00174-7.
[39] K. H. Chu, B. C. Tan, Is the Frumkin (Fowler–Guggenheim) adsorption isotherm a two- or three-parameter equation?, *Colloid and Interface Science Communications*, 2021, **45**, 100519, doi: 10.1016/j.colcom.2021.100519.
[40] M. Lovrić, Simulation of the adsorption–desorption hysteresis for Frumkin isotherm, *Adsorption*, 2024, **30**, 957-964, doi: 10.1007/s10450-024-00480-9.
[41] N. Ayawei, A. N. Ebelegi, D. Wankasi, Modelling and interpretation of adsorption isotherms, *Journal of Chemistry*, 2017, **2017**, 3039817, doi: 10.1155/2017/3039817.
[42] M. Abdel Salam, M. Mokhtar, S. M. Albukhari, D. F. Baamer, L. Palmisano, M. Jaremko, M. R. Abukhadra, Synthesis and characterization of green ZnO@polynaniline/bentonite tripartite structure (G.Zn@PN/BE) as adsorbent for as (V) ions: integration, steric, and energetic properties, *Polymers*, 2022, **14**, 2329, doi: 10.3390/polym14122329.
[43] S. Shimizu, N. Matubayasi, Fluctuation adsorption theory: quantifying adsorbate–adsorbate interaction and interfacial phase transition from an isotherm, *Physical Chemistry Chemical Physics*, 2020, **22**(48), 28304-28316, doi: 10.1039/D0CP05122E.
[44] L. Zhang, H. A. Loáiciga, M. Xu, C. Du, Y. Du, Kinetics and mechanisms of phosphorus adsorption in soils from diverse ecological zones in the source area of a drinking-water reservoir, *International Journal of Environmental Research and Public Health*, 2015, **12**(11), 14312-14326, doi: 10.3390/ijerph121114312.
[45] N. Hasani, T. Selimi, A. Mele, V. Thaçi, J. Halili, A. Berisha, M. Sadiku, Theoretical, equilibrium, kinetics and thermodynamic investigations of methylene blue adsorption onto lignite coal, *Molecules*, 2022, **27**(6), 1856, doi: 10.3390/molecules27061856.
[46] S. Kurajica, I. Minga, R. Blazic, K. Muzina, P. Tominac, Adsorption and degradation kinetics of methylene blue on As-prepared and calcined titanate nanotubes, *Athens Journal of Sciences*, 2018, **5**, 7-22, doi: 10.30958/ajs.5-1-1.
[47] Y. Li, B. Zhao, T. Shang, Adsorption of copper(II) in biochar-humic acid–water system, *Scientific Reports*, 2025, **15**, 24948, doi: 10.1038/s41598-025-09880-5.
[48] D. Wang, R. Wang, W. Peng, J. Zhang, Y. Wang, M. Huang,

N. Zhang, Y. Duan, Y. Fang, Experimental and DFT study of Cu(II) removed by Na-montmorillonite, *Water Science and Technology*, 2023, **87**, 834-851, doi: 10.2166/wst.2023.045.
[49] G. Wu, B. Wang, C. Xiao, F. Huang, Q. Long, W. Tu, S. Chen, Effect of montmorillonite modified straw biochar on transfer behavior of lead and copper in the historical mining areas of dry-hot valleys, *Chemosphere*, 2024, **352**, 141344, doi: 10.1016/j.chemosphere.2024.141344.
[50] R. Katiyar, A. K. Patel, T.-B. Nguyen, R. R. Singhania, C.-W. Chen, C.-D. Dong, Adsorption of copper (II) in aqueous solution using biochars derived from Ascophyllum nodosum seaweed, *Bioresource Technology*, 2021, **328**, 124829, doi: 10.1016/j.biortech.2021.124829.
[51] İ. Teğin, S. Öc, C. Saka, Adsorption of copper (II) from aqueous solutions using adsorbent obtained with sodium hydroxide activation of biochar prepared by microwave pyrolysis, *Biomass Conversion and Biorefinery*, 2025, **15**, 6805-6816, doi: 10.1007/s13399-024-05477-6.